Exp Astron
https://doi.org/10.1007/s10686-018-9599-9

ORIGINAL ARTICLE

Soft proton flux on *ATHENA* focal plane and its impact on the magnetic diverter design

Simone Lotti[1] · Teresa Mineo[2] · Christian Jacquey[3] · Monica Laurenza[1] · Valentina Fioretti[4] · Gabriele Minervini[1] · Giovanni Santin[5] · Silvano Molendi[6] · Tommaso Alberti[1] · Paolo Dondero[7] · Alfonso Mantero[7] · Vladimir Ivanchencko[8] · Claudio Macculi[1] · Luigi Piro[1]

Received: 7 March 2018 / Accepted: 10 July 2018

Abstract The experience gained with the current generation of X-ray telescopes like *Chandra* and *XMM-Newton* has shown that low energy "soft" protons can pose a severe threat to the possibility to exploit scientific data, reducing the available exposure times by up to 50% and introducing a poorly reproducible background component. These soft protons are present in orbits outside the radiation belts and enter the mirrors, being concentrated towards the focal plane instruments, losing energy along their path and finally depositing their remaining energy in the detectors. Their contribution to the residual background will be even higher for *ATHENA* with respect to previous missions, given the much higher collecting area of the mirrors, even if the instruments will likely suffer no significant radiation damage from this particles flux. As a consequence this soft proton flux shall be damped with the use of a magnetic

This work is supported by the ESA "*AREMBES*" Contract No 4000116655/16/NL/BW.

✉ Simone Lotti
simone.lotti@iaps.inaf.it

[1] INAF-IAPS Roma, Via Fosso del Cavaliere 100, Rome, 00133, Italy

[2] INAF-IASF Palermo, Via Ugo la Malfa 153, 90146 Palermo Italy

[3] IRAP/CDPP Toulouse, 9, avenue du Colonel Roche, Toulouse France

[4] INAF-OAS Bologna, Via Piero Gobetti, 101, 40129 Bologna Italy

[5] ESA/ESTEC and RHEA System, Keplerlaan 1, 2201 AZ Noordwijk, Netherlands

[6] INAF-IASF Milano, Via E. Bassini 15, I-20133 Milano Italy

[7] SWHARD srl, Via Greto di Cornigliano, 6, 16152 Genova Italy

[8] Tomsk State University, Lenin Ave, 36, Tomsk, Russia

Published online: 14 August 2018

diverter to avoid excess background loading on the *WFI* or *X-IFU* instruments. We present here a first complete evaluation of this background component for the two focal plane instruments of the *ATHENA* mission in absence of a magnetic diverter, and derive the requirements for such device to reduce the soft protons induced background below the level required to enable the mission science. We estimate the soft proton flux expected in L2 for the interplanetary component and for the component generated locally by acceleration processes in the magnetotail. We produce a proton response matrix for each of the two instruments of *ATHENA* focal plane, exploiting two independent Monte Carlo simulations to estimate the optics concentration efficiency, and Geant4 simulations to evaluate the energy loss inside the radiation filters and deposited in the detector. With this modular approach we derive the expected fluxes and spectra for the soft protons component of the background. Finally, we calculate the specifics of a magnetic diverter able to reduce such flux below the required level for both *X-IFU* and *WFI*.

Keywords *ATHENA* · X-ray · Background · Monte Carlo · Geant4 · Space environment · Soft protons · Ray-tracing

1 Introduction

When the first *XMM-Newton* datasets became available, sudden and intense increases of the background level observed by the pn and MOS detectors were discovered (see Fig. 1). These "flares" were totally unrelated to background rates measured by the radiation monitor onboard *XMM-Newton*, and were eventually associated to protons of energies in the few tens to few hundreds of keV [23], the so-called "soft protons". These soft protons flares increased the backgound level by several orders of magnitude for a fraction of the observing time close to 50%, forcing to discard nearly half of the scientific data.

After some time, it was understood that, in addition to this flaring component, also existed a quiescent soft proton component with poorly reproducible spectrum and intensity contaminating data at all times that could constitute from 1/10 to 1/3 of the cosmic ray (CR) component [11, 19]. These low energy particles thus limited the exploitation of the data in two significant ways: firstly by reducing exposure times by about 40-50% of time [20], and secondly by contaminating the remaining data with a subdominant but poorly reproducible background component [21].

Soft protons interact with the X-ray optics in a similar way to photons, and as a consequence are funnelled towards the focal plane where they impact the detectors. Given the larger collecting area of the *ATHENA* mirrors with respect to *XMM-Newton*, we expect their contribution to be even more significant. The challenging scientific goals of the mission, such as the observation of faint/diffuse/distant sources such as distant AGNs or galaxy clusters outskirts, impose strong requirements on the level of the non X-ray background (NXB), and the soft protons induced background can contribute up to a maximum of 10% (that corresponds to a flux of 5×10^{-4} cts

cm^{-2} s^{-1} keV^{-1} in the 2-10 keV energy band). The solution is to introduce a high magnetic field between the mirrors and the detectors to deflect these particles away from the instruments field of view (FoV).

In this paper, we will address the problems of estimating the soft proton flux on the *ATHENA* detectors and identifying the required features of a magnetic diverter capable of reducing this flux below the mission requirement for the soft proton flux, exploiting a modular approach: we analyze the L2 environment to understand what is the flux that will impact on the optics (Section 2); we address the telescope transmission, as for the standard X-ray spectral analysis, with a soft protons response matrix that includes the optics efficiency, the filters transmission and the energy deposited in the detectors (Section 3); and we derive the expected flux levels and spectra detected by the focal plane instruments (Section 4). Finally we calculate the features required from the magnetic diverter to damp the flux below the level required by the mission (Section 5).

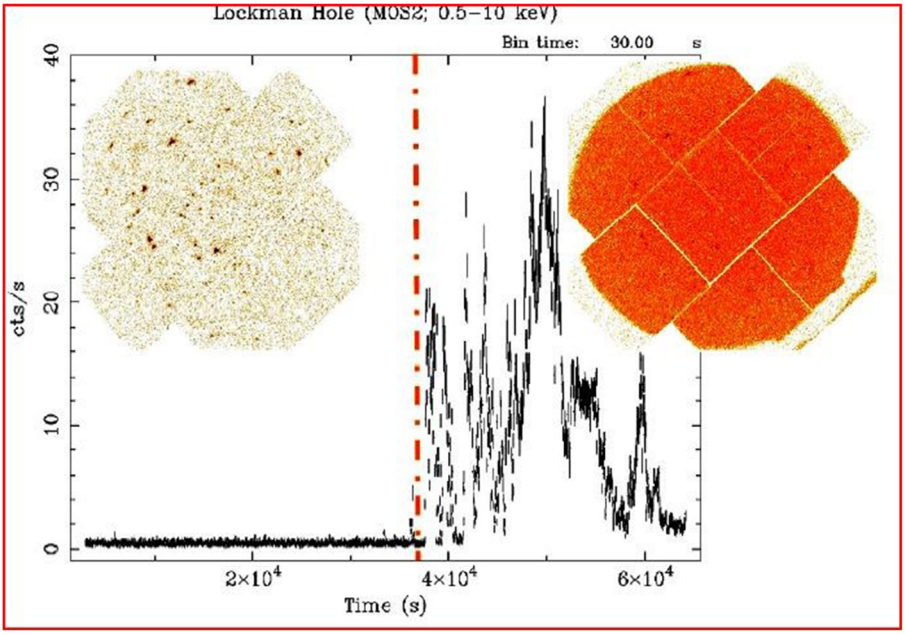

Fig. 1 An example of an EPIC observation badly affected by soft protons flares. The light curve accumulated from the full field of view shows an significant and abrupt increase in the background level some 37 ks after the beginning of the observation, with peaks up to 2 orders of magnitude above the quiescent level. Note the difference in surface brightness on the EPIC MOS between the image on the left, which was accumulated during the quiescent period and the one on the right accumulated during the flares. Most importantly, no increase in the background level is seen in the outer parts of the detector which are not exposed to radiation from the telescope [28]

Table 1 Occurrence frequency distribution versus Y distance from L2 of the different regions computed in bins of 10 R_e, as sampled from the *GEOTAIL* satellite

Y_{bin} (R_e)	N_{event}	f_{SW}	f_{MS}	f_{TA}	f_{BL}	f_{PS}	f_{LB}
−90	0	X	X	X	X	X	X
−80	0	X	X	X	X	X	X
−70	0	X	X	X	X	X	X
−60	447	0	1.0000	0	0	0	0
−50	1690	0	0.9923	0.0077	0.0077	0	0
−40	1576	0	1.0000	0	0	0	0
−30	1381	0	0.9254	0.0746	0.0529	0.0217	0
−20	4731	0	0.6540	0.3460	0.2581	0.0875	0.0004
−10	9630	0	0.6556	0.3444	0.2022	0.1281	0.0141
0	3146	0	0.3722	0.6278	0.3503	0.2486	0.0289
10	6108	0	0.1213	0.8787	0.4486	0.3991	0.0309
20	3784	0	0.2011	0.7989	0.4701	0.3021	0.0267
30	971	0	0.5850	0.4150	0.2122	0.1916	0.0113
40	1168	0	0.9050	0.0950	0.0377	0.0574	0
50	1369	0	0.9752	0.0248	0.0212	0.0037	0
60	1231	0	1.0000	0	0	0	0
70	0	X	X	X	X	X	X
80	0	X	X	X	X	X	X
90	0	X	X	X	X	X	X

This example correspond to the distant magnetotail (distance > 185 R_e from Earth). Y_{bin} designates the central value of the bins. In the table f_{SW} is the Solar Wind Occurrence frequency, f_{MS} the magnetosheath Occurrence frequency, f_{TA} the magnetotail Occurrence frequency, f_{BL} the boundary layer Occurrence frequency, f_{PS} the plasma sheet Occurrence frequency, and f_{LB} the lobe Occurrence frequency. The "X" symbol indicates that there were no records in the bins (i.e., not sampled along the orbit)

2 The L2 environment

In this section we address the external particles flux impacting on the mirrors. We make use of the results of the L2 environment analysis performed under the *AREMBES*[1] ESA contract.

To understand in which region *ATHENA* will fly we can assume for *ATHENA* the same kind of orbits around L2 exploited by Planck, Hershel and eRosita satellites at radii of 63, 100 and 157 R_e (where R_e is the Earth radius) around L2 in the plane perpendicular to the Sun-Earth direction, respectively. By looking at Table 1 we can find that *ATHENA* is expected to spend its entire lifetime inside the magnetosheath (MS) or in the solar wind (SW): we then focused on the protons spectra measured there.

[1] ATHENA Radiation Environment Models and X-Ray Background Effects Simulators

2.1 The interplanetary flux of soft protons

The interplanetary space is composed by several particle populations of different origins and characteristics (in terms of composition, energy spectrum, timing). In particular, the main energetic particles components are: 1) the suprathermal tail of the solar wind; 2) Solar Energetic particles (SEPs), which are occasionally emitted at the Sun during eruptive events; 3) galactic cosmic rays, that penetrate the heliosphere from interstellar space; 4) particle enhancements produced by transient interplanetary shock waves, e.g., driven by coronal mass ejections (CMEs); 5) particle enhancements associated with the shocks that develop at the boundaries of corotating interaction regions (CIRs), produced by the interaction between fast and slow solar wind streams.

The estimation of the energetic particles radiation environment in the interplanetary space is essential to perform an assessment study related to any scientific mission profile, as they can interact with the spacecraft and instruments. As already explained, the proton component with energy in the range 50 keV $<$ E $<$ 1 MeV (hereafter called soft protons) concentrated by the optics decreases the instrumental sensitivity.

To characterize the energetic particle environment at L2 point, we first used the proton observations recorded by the *WIND* spacecraft during its flight in the distant terrestrial magnetotail, wich provide direct estimates of the proton flux in the L2 region. We selected periods for which the *WIND* spacecraft was at distances $X > 150\ R_e$. Several soft proton enhancements were identified and compared with those simultaneously observed by the EPAM/ACE instrument in the undisturbed solar wind at L1.

We found that all the soft proton flux enhancements recorded by *ACE* at L1 are observed at L2 as well for all the considered energies. For instance, a soft proton flux enhancement was observed by *ACE* at L1 and by *WIND* in the far magnetotail on December 2003. We derived the proton fluence spectrum by integrating the data over the whole duration of the event (from 6 December 2003 at 22:55:32 UT to 8 December 2003 at 16:50:00). The obtained spectra, illustrated in Fig. 2, show that the proton fluence spectra for the L1 (*ACE* data) location are only slightly higher than those at L2 (*WIND* data) below 1 MeV. This feature has been found for several events observed at both L1 and L2. Hence, we can reasonably assume that the proton flux at L1 measured by *ACE*, whose data cover a long time period, can be used to estimate the soft protons environment at L2, at least to provide an upper limit to those of solar interplanetary origin (i.e., not produced in the Earth's magnetosphere, see next section), given that their level is sliglty higher than that at L1 (see Fig. 2).

In order to estimate the soft proton flux levels, a long term analysis of the hourly proton flux data recorded aboard the *ACE* spacecraft by the EPAM/LEMS120 instrument has been performed. The available data cover the period from August, 31 1997 to December, 31 2014, i.e., almost two solar cycles (n. 23 and n. 24).

Hourly proton flux data have been analyzed by evaluating Cumulative Distribution Functions (CDFs) for all the eight differential energy channels of the EPAM/LEMS120 experiment (0.047-4.8 MeV). The CDFs of a random variable F', or of a distribution function of F', evaluated at F, is the probability that F' will take a value less than or equal to F. The percentages of time (with respect to the total time

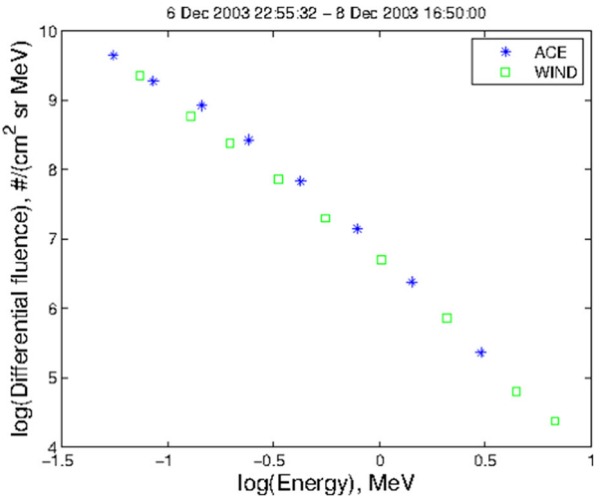

Fig. 2 Proton fluence spectra of the proton enhancement observed on December 2003, obtained with *ACE* (L1) and *WIND* (L2)

coverage) below different flux thresholds F can be easily evaluated from the CDFs for each energy channel.

The flux levels and spectra below which the measured flux lies for a given percentage of time are reported in Table 2 (third row) and Fig. 4 for the 10%, the 50% and the 90% cases.

2.2 The locally accelerated soft protons component

During active periods, the magnetosphere accumulates energy transmitted by the solar wind through its boundary, the magnetopause, where magnetic reconnection develops. This energy is first stored in the magnetotail as magnetic energy and is then explosively dissipated during perturbated events called "magnetospheric substorms". The substorms occur recurrently at a time scale of 2-3 hours, and affect the whole magnetospheric system. In the magnetotail, magnetic reconnection and current sheet acceleration processes generate important energetic particle fluxes, including electrons, protons and ions of both ionospheric (O^+) and solar (He^{2+}) origins. The enhancement of energetic ion fluxes are directly related to the development of

Table 2 Spectral shapes resulting from the fit of *GEOTAIL* and *ACE* data below 200 keV. Fluxes are in cts cm^{-2} s^{-1} keV^{-1} sr^{-1} while the energy E is in keV

	$F_{10\%}$	$F_{50\%}$	$F_{90\%}$
Quiet MS	$242 \times E^{-2.05}$	$238735 \times E^{-3.21}$	$860339 \times E^{-2.94}$
Active MS	$24980 \times E^{-2.89}$	$1.61e+6 \times E^{-3.26}$	$6.95e+6 \times E^{-3.11}$
Interplanetary SW	$4168.7 \times E^{-2.54} e^{\frac{E}{4000}}$	$44808.8 \times E^{-2.74} e^{\frac{E}{2380.9}}$	$3963.4 \times E^{-1.62} e^{\frac{-E}{3333.3}}$

substorms [8, 17, 27]. The accelerated ions then diffuse in the whole magnetotail and beyond.

STEREO [18] measurements revealed than the energetic ions accelerated during substorm could be detected inside the interplanetary medium at very large downtail distance ($> 500\ R_e$) and far away in the transverse direction ($> 500\ R_e$) from the magnetotail [25]. The *GEOTAIL* spacecraft jointly lauched by JAXA and NASA explored the distant tail and the surrounding regions during a dedicated 2 years campaign (September 1992 – October 1994). *GEOTAIL* is the unique mission having provided a long term survey of these regions. In the framework of *AREMBES* we performed a systematical analysis of the energetic ion fluxes measurement obtained by the EPIC/ICS experiment [29]. The EPIC/ICS provides the azimutal distribution (i.e., in the ecliptic plane) of the ions between 58 KeV and 3 MeV (for protons) in two polar angles at 30 degrees appart the ecliptic plane. Combining Time-Of-Flight telescopes and solid state detector, EPIC/ICS separates the detected ions into 4 groups: P (Protons), HE (Heliums), CNO (Carbon, Nitrogen, Oxygen) and H (heavier ions). The time resolution of the data used in this paper was of 96 seconds.

The data time-averaged over 5 minutes have been separated into two datasets "quiet magnetosphere" (Auroral Electrojet Index $AE < 125\ nT$) and "active magnetosphere" ($AE > 125\ nT$), with respect to the Auroral Index value used as a proxy of the geomagnetic activity. Then, for each dataset, the data have been sorted into 7 classes with respect to the region where the measurement were performed (see Table 1 and Fig. 3).

Finally, for each of these classes, the ion fluxes have been averaged on the whole distribution of azimuthal directions (omnidirectional flux) and inside four 67.5 degrees wide azimutal sectors:

- the Tailward flux of protons streaming in the antisunward direction,
- the Duskward flux of of protons streaming in the westward direction,
- the Sunward flux of protons streaming in the sunward direction,
- the Dawnward flux of of protons streaming in the eastward direction.

Given that the pointing directions of *ATHENA* are centered on the plane perpendicular to the Sun-Earth direction, for this study we take into account only the fluxes measured in the Duskward and Dawnward directions (averaged to obtain the "sideward" flux) in the magnetosheath region.

The *AREMBES* analysis provided the flux thresholds below which the *GEOTAIL* satellite measured flux lies for a given percentage of time, and we took into account the 10%, the 50% and the 90% cases (see Table 2 and Fig. 4). It must be noted that the lowest energy measured by *GEOTAIL* is $\sim$ 58 keV, while we extended the fitted spectrum down to few keV in order to be able to dive into the energy range useful for our calculations.

3 *ATHENA* soft proton response matrix

A response matrix used to deconvolve the observed spectra and determine the physical parameters of the source emission is a common tool in the standard X-ray

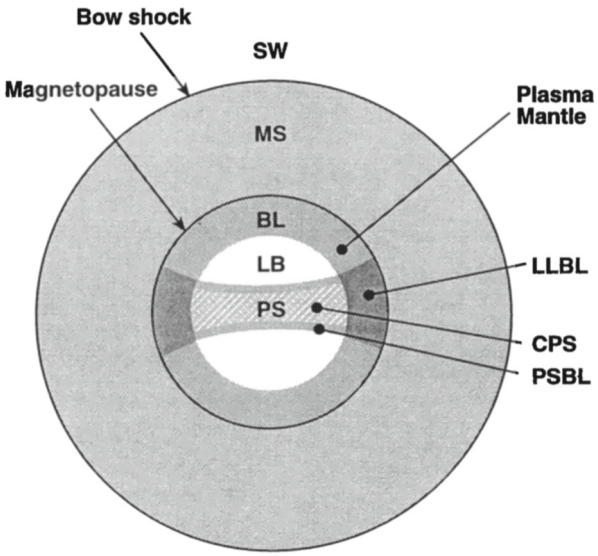

Fig. 3 Cross-section of the magnetotail and surrounding regions [13]. In the figure SW indicates the solar wind; MS the magnetosheath; LB the lobe; BL the boundary layer including plasma mantle and low-latitude boundary layer (LLBL); PS is the plasma sheet, including central plasma sheet (CPS) and plasma sheet boundary layer (PSBL)

data analysis. Spectral fitting are, in fact, generally performed with XSPEC [12] an interactive X-ray spectral-fitting program opportunely designed to be detector-independent, in which response matrices take care of the instrument characteristics.

A first attempt to produce a response matrix to analyse XMM-Newton data of flaring events due to soft protons has been presented by [22]. This matrix allows us for a study of the environmental characteristic of the Earth magnetosphere crossed by the satellite orbits with a precision mainly limited by systematics in the theoretical models for the interaction of protons with all the telescope components. Considering the flexibility of this tool, we decided to use response matrices in computing the rates and the spectra due to soft proton contaminations for the *ATHENA* focal plane instruments. This was easily performed within XSPEC with the command FAKEIT that creates simulated spectra from any given theoretical model.

The format of the response matrix, as defined by the Office of Guest Investigators Program (OGIP) for high-energy astrophysics projects, is Flexible Image Transport System (FITS) conform to the OGIP Calibration Memo CAL/GEN/92-0021.[2] In analogy with X-ray analysis, the proton response matrix contains the probability that an incoming proton of energy E is detected in the output detector channel PHA. It is composed of two FITS files: *i)* the ancillary response file (*arf*) with the effective area computed as the product of the telescope grasp, the filter transmission and the probability that an absorbed proton is detected in the working energy ranges of the *ATHENA* instruments; *ii)* the detector redistribution matrix file (*rmf*) that stores in

[2] http://heasarc.gsfc.nasa.gov/docs/heasarc/caldb/docs/memos/calgen92002/calgen92002.html

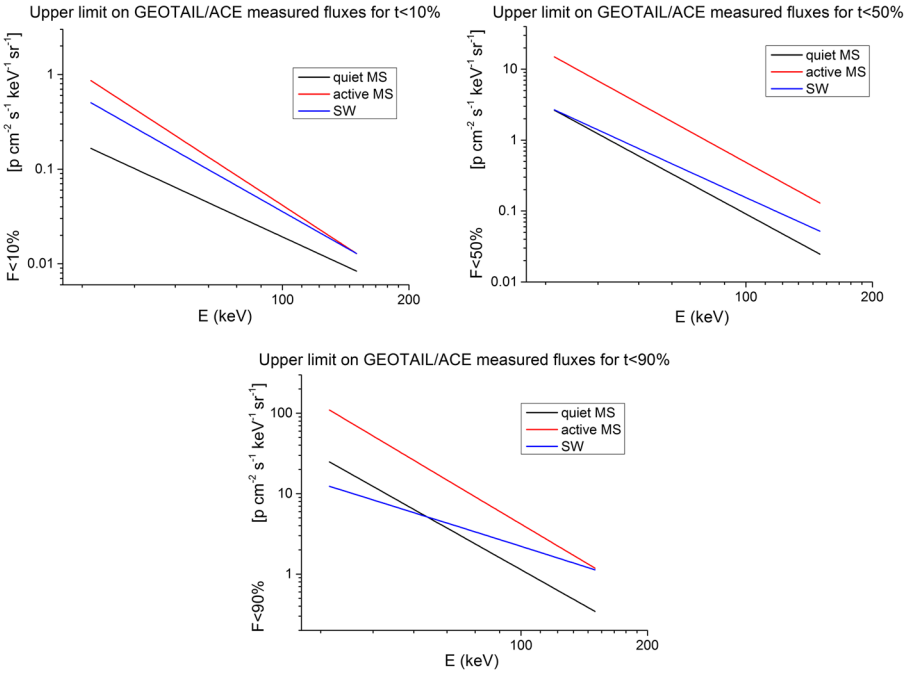

Fig. 4 The maximum fluxes measured by *GEOTAIL* and *ACE*, for a given fraction of the time spent in each zone

a 2-d array (energy vs PHA channel) the probability that a proton with energy E_i is detected in the channel PHA correspondent to the energy E_o.

The X-IFU matrix has 500 rows each correspondent to an input proton energy uniformly distributed in the range 27–400 keV and 512 PHA output channels uniformly distributed in the range 0.2-12 keV. The WFI matrix has 81 rows with 1 keV step energies in the range 19–100 keV and 512 PHA output channels uniformly distributed in the range 0.1-15 keV.

In the following subsections we present in detail the physical models of the proton interactions with the mirror shells, the filters and the detectors adopted in the production of the response matrices, together with the check we performed to test the results.

3.1 Mirror simulator

The mirror contribution to the telescope efficiency is introduced in the *arf* file with the grasp $G(\vartheta, E)$ defined as:

$$G(\vartheta, E) = 2\,\pi \int_0^{\vartheta_{max}} A(\vartheta, E)\ \sin\deg\vartheta\ d\vartheta \tag{1}$$

where E is the proton energy, $A(\vartheta, E)$ the effective area at the incident angle ϑ and $[2\,\pi\ \sin\deg\vartheta\ d\vartheta]$ is the differential solid angle integrated up to the maximum off-axis angle ϑ_{max}.

This function was obtained independently with two different codes: a ray-tracing and a Geant4 [1–3] based simulator. The ray-tracing is a Monte Carlo stand alone code able to simulate either photons or protons. It is a modified version of on a existing code used for the on-ground and in-flight calibration of the photon effective area of the X-ray telescopes BeppoSAX [9] and Swift [10]. It follows the particle through the interactions with the mirror shells up to the focal plane taking into account the geometry of the optics and the effects of the mounting system for the SPO plates. Pores are included in the simulator assuming that all protons that interact with the uncoated surfaces are stopped; this is equivalent to the assumption that these protons are scattered far from the detector region. The Remizovich proton reflection model implemented in the ray-tracing code was derived by [26] solving the transport equation for glancing incident ion beams in the diffusion approximation under the assumption of almost elastic reflection. The adopted formula is given in [22].

Independent Geant4 simulations of soft proton scattering have been carried out as part of the ESA/*AREMBES* project activities with the aim of validating the proposed physics models for proton scattering at grazing angles. Using both Coulomb scattering and the Remizovich solution, in the approximation of no energy losses, the Geant4 simulated scattering efficiency is compared in [14, 16] to laboratory measurements (for proton energies $>$ 250 keV). Both models confirm the peak in scattering probability at specular angles, and are well consistent with the measurements for scattering angles $>$ 1 degree. For smaller angles, the Remizovich model predicts a scattering probability more than twice what obtained by using Coulomb scatterings. The Geant4 mass model of the full ATHENA SPO has also been developed, using conical approximations to build the paraboloid-hyperboloid Wolter-I sections. Such approximations reduce by 20% the total proton transmission with respect to the use of the exact SPO design implemented in the ray-tracing simulator. See [15] for a detailed description of the mass model.

A detailed comparison between the Geant4 code and the ray-tracing results showed an agreement in the transmission factors at level of $\sim$ 10%.

The mirror response introduced in the response matrix was computed with the ray-tracing code, assuming a Wolter 1 mirror profile with 12 m focal length and $\sim$2 m^2 effective area at 1 keV. Pores have 1 mm azimuthal width, 0.605 mm radial width and 0.17 mm septal thickness. The proton reflection is computed using the Remizovich model that is the most efficient reflection model we investigated [14]. To compute *ATHENA* grasp, proton incident directions are uniformly generated in a solid angle with a maximum off-axis of 5° and events reaching the focal plane are considered if they are contained in a 2.5′ and 20′ radius circle for X-IFU and WFI, respectively.

3.2 Filters and detector simulator

After being funnelled by the *ATHENA* SPO the soft protons will cross the filters of the two focal plane instruments, losing a fraction of their energy inside them and will eventually be detected by the instruments. To compute the effects of the filters and the detection efficiencies, we use ad-hoc Geant4 Monte Carlo simulations where the filter and the detectors are opportunely modelled.

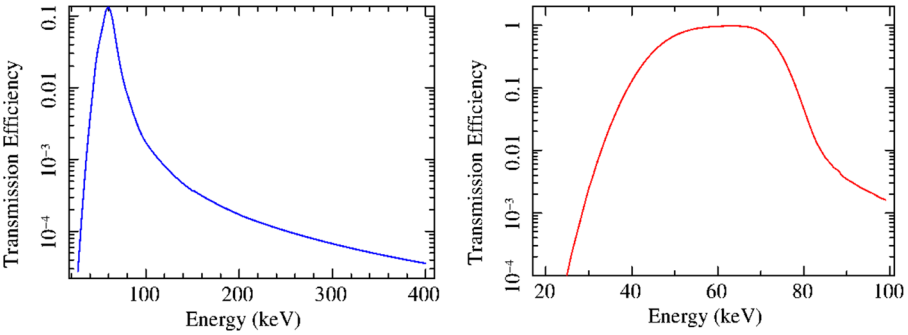

Fig. 5 Transmission efficiency for the *X-IFU* (left, blue) and *WFI* (right, red) filters computed as the probability that a proton crossing the filter is detected in the energy working range of the detectors

The *X-IFU* design includes 5 thermal filters of identical thickness whose baseline foreseen a total of 0.28 μm Kapton filter and 0.21 μm Aluminum mesh [4]; the detector is simulated as a 1 μm Au - 4 μm Bi bilayer, as in the real case. The *WFI* [7] will also be equipped with filters to block the optical-UV contamination. They are composed by a Kapton mesh of 0.35 μm plus an Aluminum layer of 0.04 μm thickness. The detector mass model implemented in Geant4 is composed by 4 different layers: 0.07 μm Aluminum, 0.035 μm Silicon Nitrate, 0.035 μm Silicon Dioxide and 450 μm Silicon.

To compute the effects of the filters we shoot a flat spectrum of protons between 1 and 150 keV towards the detectors and derive the filter transmissions as the probability that an event crossing the filter is detected in the energy working range of the two instruments; the transmission functions used in the matrix are plotted in Fig. 5.

In the *X-IFU* simulation the five filters were modeled separately with different radii and distances from the detector [4], while in the *WFI* simulations a simple multilayer slab geometry is considered without any separation between the filter and the detector. In both simulation sets, protons were shot perpendicularly to the highest surface considering that the incident angles of the focused protons were small enough (a few degree from the optical axis) to consider this approximation correct.

The filters design is however still under development, an updated design for the optical filters can be found in [5, 6]; the differences in the transmitted fraction of soft protons with respect to the currently simulated setup is below a factor of 3.

The interaction with the detector is included in the *rmf* file where each row was built with the Geant4 simulation using mono-energetic beams of protons and considering the energy deposited in the detector working energy range after crossing the filters. The number of input events is varied in order to have similar output statistics for all input energies. The accumulated spectra were then normalised to one as required by the format of the matrix, being all efficiency included in the *arf* file.

The redistribution matrix relative to the input proton energy of 60 keV for the *X-IFU* (left panel) and the *WFI* (right panel) is shown in Fig. 6.

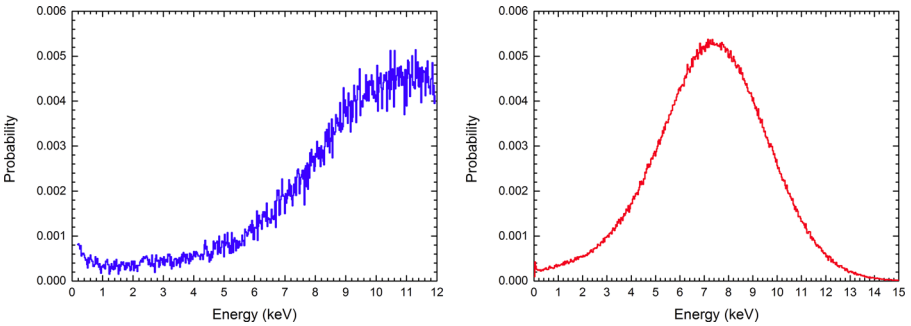

Fig. 6 Row of the redistribution matrix relative to the input proton energy of 60 keV for the *X-IFU* (left, blue) and the *WFI* (right, red)

4 The expected fluxes at the focal plane and the requirements for the magnetic diverter

Using the response matrices and the tool FAKEIT within XSPEC, we derive the expected fluxes and spectra of soft protons at the focal plane level in absence of a magnetic diverter, compare it to the desired background level, and derive the required efficiency of the diverter. Integrating these spectra over the whole energy range we can find the total flux expected on the *X-IFU* and on the *WFI*. Table 3 presents the rates detected in the energy range 2-10 keV by the two focal plane instruments for each of the considered L2 input spectrum, and Figs. 7, 8 and 9 the corresponding spectra. The different shape of the detected spectra in the two detectors is due to the different filters configuration (see Figs. 10 and 6). As an example, the spectra of initial energies of the soft protons that reach the focal plane with $2 < E_{FPA} < 10$ keV are plotted in Fig. 10 for *X-IFU* and *WFI*.

The requirement on the level of background induced by soft protons on the focal plane instruments is 10% of the background induced by GCR for 90% of time, i.e., 5×10^{-4} cts cm^{-2} s^{-1} keV^{-1}. As a consequence, the soft protons induced background in the energy range 2–10 keV should not exceed 4×10^{-3} cts cm^{-2} s^{-1}.

We take into account the worst case among the ones shown in Table 3, that is the active magnetosheath for the 90% input flux. In this case it is necessary to block

Table 3 Integrated fluxes expected on the *X-IFU* and *WFI* for the different environments described in Section 2

	X-IFU			*WFI*		
	$F_{10\%}$	$F_{50\%}$	$F_{90\%}$	$F_{10\%}$	$F_{50\%}$	$F_{90\%}$
Quiet MS	0.0001	0.001	0.01	0.001	0.01	0.13
Active MS	0.0004	0.006	0.04	0.004	0.07	0.52
SW	0.0003	0.001	0.01	0.003	0.01	0.11

Fluxes are expressed in cts cm^{-2} s^{-1}

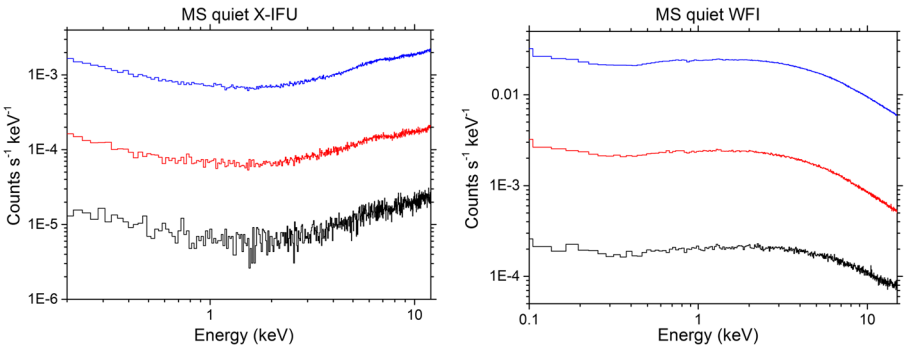

Fig. 7 Detected spectra for the 10%, 50% and 90% levels for *X-IFU* (left) and the *WFI* (right) relative to the Quiet MS

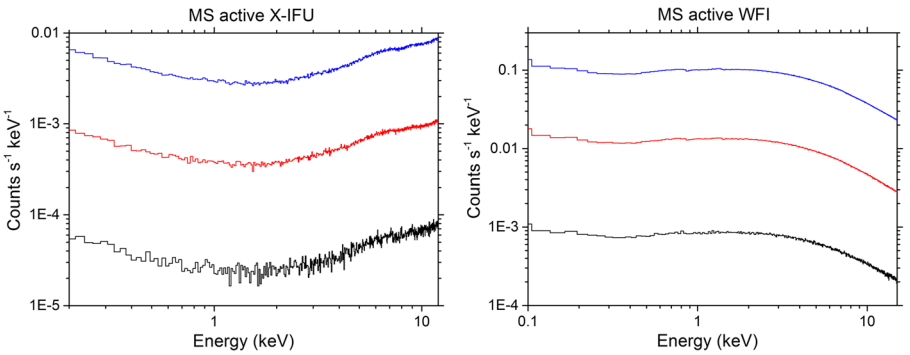

Fig. 8 Detected spectra for the 10%, 50% and 90% levels for *X-IFU* (left) and the *WFI* (right) relative to the Active MS

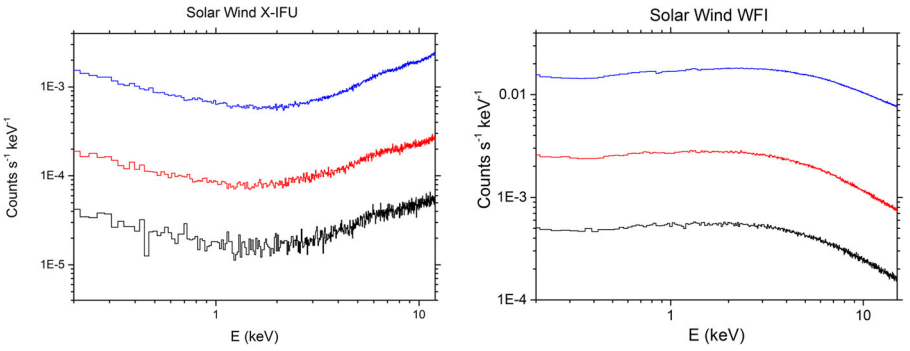

Fig. 9 Detected spectra for the 10%, 50% and 90% levels for *X-IFU* (left) and the *WFI* (right) relative to the Solar Wind

$\sim$ 90% of the incoming flux for *X-IFU* and $\sim$ 99% for the *WFI*. If we look at the cumulative curve for this spectrum (see Fig. 11) we can see that this corresponds to blocking protons with energies up to $\sim$ 66 keV for the X-IFU and up to $\sim$ 76 keV for the WFI.

5 The required efficiency of the magnetic diverter

In the following we will derive the requirement for the magnetic field B of the *ATHENA* Magnetic Diverter (MD). We refer to the Halbach configuration, which is the current ESA baseline for the *ATHENA* magnetic diverter. We take into account the worst case of a proton entering the MD from the edge of the optics to the opposite side of the MD. For the *X-IFU* the requirement is set by the necessity to deflect a $\sim$ 66 keV proton outside the entrance window of the cryostat, while for the *WFI* the requirement is defined by the necessity to deflect a $\sim$ 76 keV proton outside the instrument area. The problem is schematized in Fig. 12.

The MD inner diameter d_0 is determined by its distance from the focal plane, L_0 and the angle γ, given that the projection of the MD on the focal plane is supposed to be at least equal to the detector diagonal:

$$d_0 = D - 2L_1 tan(\gamma) \tag{2}$$

A particle that comes from the edge of the optics will enter the MD on its opposite edge with an angle

$$\alpha = -arctan\frac{D + d_0}{2L_1} \tag{3}$$

Assuming that the particle will cross the MD in a time $t = L_0/v$, the deflection angle will be:

$$\theta = \frac{qBL_0}{mv} \tag{4}$$

and therefore the particle will exit the MD with an angle

$$\beta = \alpha + \theta \tag{5}$$

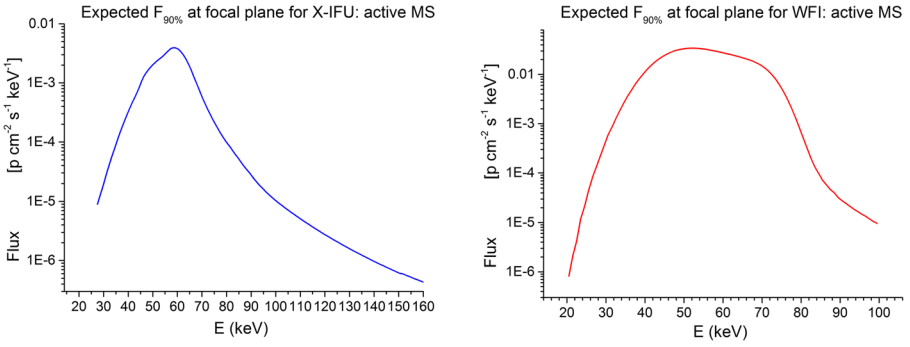

Fig. 10 Spectra of initial energies of the protons that reach the focal plane with $2 < E_{FPA} < 10$ keV for the worst case of active magnetosheath (90% of time) for X-IFU (left) and WFI (right)

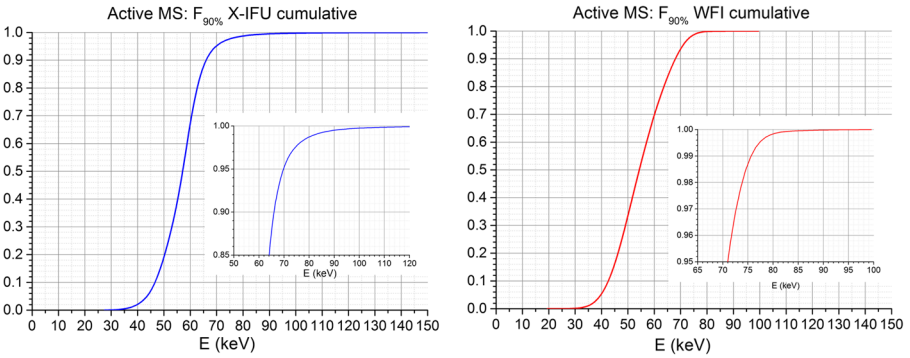

Fig. 11 Cumulative curves of the incoming flux on the focal plane instruments for the worst case of active magnetosheath (90% of time), *X-IFU* (left) and WFI (right)

We define β^* as the angle subtended by the detector, representing the critical angle for a particle to be deflected:

$$\beta^* = arctan(\frac{d + L_2 tan(\gamma)}{L_2}) \tag{6}$$

In the case of the *X-IFU* detector, we need to deflect the 66 keV particles outside the cryostat baffle. The entrance aperture of this baffle has a diameter of 21.9 cm and extends above the focal plane for 80 cm. Varying the linear size of the diverter, from $L_0 = 18$ cm up to $L_0 = 5$ cm, and its position, from $L_2 = 1.6$ m up to $L_2 = 1$ m,

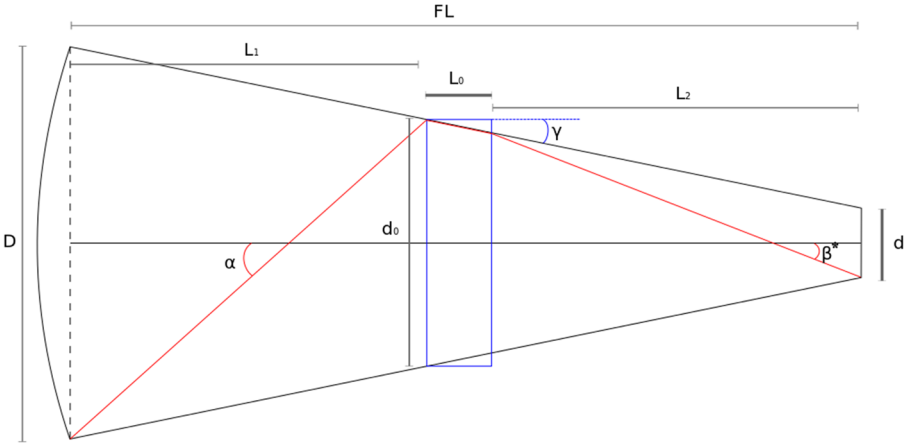

Fig. 12 Schematic of the magnetic diverter, where: FL is the focal length of the telescope; L_0 is the MD height along the line of sight; L_1 is the distance of the MD from the mirrors; L_2 is the distance of the MD from the FP; D is the optics diameter; d is the detector diagonal; d_0 is the inner radius of the MD, given γ it will depend on $L_1 = FL - L_2 - L_0$; α is the angle from the edge of the optics to the MD; β^* is the critical angle from the edge of the MD to the opposite side of the detector. (Particles exiting the MD with angles higher than β will not intercept the detector); γ is the angle from the edge of the optics to the detector

we range a magnetic field B as:

$$B = \begin{cases} 0.12\ T & \text{for } L_0 = 18\,\text{cm and } L_2 = 1.6\,\text{m} \\ \\ 0.78\ T & \text{for } L_0 = 5\,\text{cm and } L_2 = 1\,\text{m} \end{cases} \tag{7}$$

For the *WFI*, we need to deflect the 76 keV particles outside the detector area (diameter$\sim$ 21.2 cm). Varying the linear size of the diverter as we did for the *X-IFU* case, we range a magnetic field B as:

$$B = \begin{cases} 0.1\ T & \text{for } L_0 = 18\,\text{c m and } L_2 = 1.6\,\text{m} \\ \\ 0.4\ T & \text{for } L_0 = 5\,\text{cm and } L_2 = 1\,\text{m} \end{cases} \tag{8}$$

6 Summary and conclusions

We have estimated the soft proton induced background component for both *ATHENA* focal plane instruments. We adopted a modular approach: in Section 2 we determined the particle environment in wich *ATHENA* will dwell, and derived the incident proton spectra expected from the available experimental data (see Table 2). In Section 3 we created response matrices for both the focal plane instruments, to describe the soft protons interaction with the optics, the filters and the detectors. In Section 4 we exploited these information to calculate the background induced by soft protons on the focal plane detectors in all the considered environments: With the present assumptions we expect, as worst case, a 2-10 keV rate of 4×10^{-2} cts cm^{-2} s^{-1} for the *X-IFU* and 0.52 cts cm^{-2} s^{-1} for the *WFI*. Due to the energy lost inside the radiation filters and to the narrow energy band of the instruments, the major contribution is given by protons with intermediate energies: $\sim$ 80% of the contribution on the is given by protons with $45 \leq E \leq 65$ keV on both instruments. We remark that the optics, the filters configuration, and the protons reflectivity models are still under discussion and can be subjected to changes in the future.

The level of background induced by soft protons on the focal plane instruments is required to not exceed 4×10^{-3} cts cm^{-2} s^{-1} in the 2–10 keV energy band, so it is mandatory to adopt solutions to reduce or discriminate the flux at the focal plane level. The standard solution, already used to deflect electrons in the *XMM-Newton* and *Swift* missions [24, 30], is to deflect the charged particles away from the field of view of the instruments using a strong magnetic field.

In Section 5 we developed a simple model of such magnetic diverter and calculated the magnetic field necessary to reduce the background below the requirement: from this model we found that increasing the diverter linear size L_0 reduces the required B since the particles experience it for a longer flight time, while decreasing the distance of the MD from the focal plane L_2 increases the required deflection angle and thus the required B.

Results presented in Section 4 showed that it is necessary to reject protons with energies up to $\sim$ 66 keV for the *X-IFU* and up to $\sim$ 76 keV for the *WFI*, and this

requires a magnetic field in the 0.12-0.78 T range for the *X-IFU* and in the 0.1-0.4 T for the *WFI* (the exact value depending on the geometry of the system).

We remark however that the optics, the filters configuration, and the protons reflectivity models are still under discussion and can be subjected to changes in the future. In particular, considering that the model for the proton reflectivity used in this paper assumes an efficiency higher that the measured one, a reduction up to a factor four could be achieved if the next lab measurements foreseen in the ESA contract EXACRAD will validate the Coulomb scattering as best model [14]. Conversely, the updated design for the optical filters based on thinner filters [5, 6] would produce an increase of the soft proton rate up to a factor three depending on the incident spectrum. We then think that the need of introducing a proton diverter in ATHENA design coming from the results of this paper cannot be easily overtaken.

Acknowledgements GEOTAIL/EPIC data have been provided by the Applied Physics Laboratory at John Hopkins University, Laurel, MD, USA. The GEOTAIL data analysis was partly performed with the AMDA science analysis system provided by the Centre de Données de la Physique des Plasmas (CDPP http://cdpp.eu/) supported by CNRS, CNES, Observatoire de Paris and Université Paul Sabatier, Toulouse.

References

1. Agostinelli, S., Allison, J., Amako, K.: Geant4—a simulation toolkit. NIMA **506**(3), 250–303 (2003)
2. Allison, J., Amako, K., Apostolakis, J.: Recent developments in Geant4. NIMA **835**, 186–225 (2016)
3. Allison, J., Amako, K., Apostolakis, J.: Geant4 developments and applications. IEEE Trans. Nucl. Sci. **53**(1), 270–278 (2006)
4. Barbera, M., Collura, A., Gatti, F.: Baseline design of the thermal blocking filters for the X-IFU detector on board ATHENA. Proc. SPIE **9144**(91445U), 11 (2014)
5. Barbera, M., Argan, A., Bozzo, E., et al.: Thermal filters for the ATHENA X-IFU: Ongoing activities toward the conceptual design. JLTP **184**, 706–711 (2016). https://doi.org/10.1007/s10909-016-1501-4. ISSN: 0022-2291
6. Bozzo, E., Barbera, M., Genolet, L., et al.: The filter wheel and filters development for the X-IFU instruments onboard Athena. In: Proceedings of SPIE, 9905, art. no. 990561. https://doi.org/10.1117/12.2232328 (2016)
7. Barbera, M., Branduardi-Raymont, G., Collura, A., et al.: The optical blocking filter for the ATHENA wide field imager: Ongoing activities towards the conceptual design. Proc. SPIE, 9601. https://doi.org/10.1117/12.2189326 (2015)
8. Christon, S.P., Gloeckler, G., Williams, et al.: Energetic atomic and molecular ions of ionospheric origin observed in distant magnetotail flow-reversal events. Geophys. Res. Lett. **21**(25), 3023–3026 (1994). (ISSN 0094-8276)
9. Conti, G., Mattaini, E., Santambrogio, E.: X-ray characteristics of the Italian X-ray astronomy satellite (SAX) flight mirror units. Proc. SPIE **2279**, 101–109 (1994). https://doi.org/10.1117/12.193179
10. Cusumano, G., Campana, S., Romano, P.: In-flight calibration of the swift XRT effective area, in gamma-ray bursts in the swift era. Nousek Am. Instit. Phys. Conf. Series **836**, 664–667 (2006). https://doi.org/10.1063/1.2207972
11. De Luca, A., Molendi, S.: The 2-8 keV cosmic X-ray background spectrum as observed with XMM-Newton. A&A **419**, 837–848 (2004)
12. Dorman, B., Arnaud, K.A.: Redesign and Reimplementation of XSPEC. Payne Astron. Soc. Pacific Conf. Series **238**, 415 (2001)
13. Eastman, T.E., Christon, S.P., Doke, T., et al.: Magnetospheric plasma regimes identified using Geotail measurements 1. Regime identification and distant tail variability. J. Geophys. Res. **103**(A10), 23503–23520 (1998). https://doi.org/10.1029/98JA01915. (JGR Homepage)

14. Fioretti, V., Mineo, T., Bulgarelli, A.: Geant4 simulations of soft proton scattering in X-ray optics - A tentative validation using laboratory measurements. Experimental Astronomy. https://doi.org/10.1007/s10686-017-9559-9 (2017)
15. Fioretti, V. et al.: The Geant4 mass model of the ATHENA silicon pore optics and its effect on soft proton funneling. Proc. SPIE, in prep (2018)
16. Guzmán, A., Perinati, E., Diebold, S., Tenzer, C., Santangelo, A.: A revision of soft proton scattering at grazing incidence and its implementation in the GEANT4 toolkit. Exper. Astron. **44**(3), 401–411 (2017). https://doi.org/10.1007/s10686-017-9537-2
17. Jacquey, C., Williams, D.J., McEntire, R.W., et al.: Tailward energetic ion streams observed at approximately 100 R(sub E) by GEOTAIL-EPIC associated with geomagnetic activity intensification. Geophys. Res. Lett. **21**(25), 3015–3018 (1994). (ISSN 0094-8276)
18. Kaiser, M.L., Kucera, T.A., Davila, J.M., Cyr, O.C.S.t., Guhathakurta, M., Christian, E.: The STEREO mission: An introduction. Space Sci. Rev. **136**(1–4), 5–16 (2008)
19. Kuntz, K.D., Snowden, S.: The X-ray-emitting components toward l = 111: The local hot bubble and beyond. ApJ **674**, 209–219 (2008)
20. Kuntz, K.D.: Presentation at IACHEC meeting (2014)
21. Leccardi, A., Molendi, S.: Radial temperature profiles for a large sample of galaxy clusters observed with XMM-Newton. A&A **486**, 359–373 (2008)
22. Mineo, T., Lotti, S., Molendi, S., Ghizzardi, S.: An XMM-Newton proton response matrix. Experimental Astronomy, in press (2017)
23. Molendi, S.: Presentation at XMM Radiation Environement Workshop (2000)
24. Nartallo, R. et al.: Radiation environment induced degradation on Chandra and implications for XMM, ESA Report Esa/estec/tos-em/00-015/RN
25. Opitz, A., Sauvaud, J.-A., Klassen, A., Gomez-Herrero, R., Bucik, R., Kistler, L.M., Jacquey, C., Luhmann, J., Mason, G., Kajdic, P., Lavraud, B.: Solar wind control of the terrestrial magnetotail as seen by STEREO. J. Geophys. Res. Space Phys. **119**, 63426355 (2014). https://doi.org/10.1002/2014JA019988
26. Remizovich, V.S., Ryazanov, M.I., Tilinin, I.S.: Energy and angular distributions of particles reflected in glancing incidence of a beam of ions on the surface of a material. Soviet J. Exper. Theor. Phys. **52**, 225 (1980)
27. Rouquette, S., Jacquey, C., Le Contel, O., et al.: Fast tailward stream observed in the distant tail associated with substorm: A multi-instrument study. Geophys. Res. Lett. **27**(21), 3571–3574 (2000)
28. Tiengo, A.: Constraining long-term and spatial variability of the pn low energy response with RXJ1856
29. Williams, D.J.: GEOTAIL energetic particle and ion composition instrument. J. Geomag. Geoelectr. **46**, 39 (1994)
30. Willingale, R.: An electron diverter for the Swift telescope, XRA study note XRT-LUX-RE-011/1. University of Leicester (2000)